Synchrotron Radiation News

ISSN: 0894-0886 (Print) 1931-7344 (Online) Journal homepage: https://www.tandfonline.com/loi/gsrn20

Imaging with Coherent Synchrotron Radiation: X-ray Imaging and Coherence Beamline (I13) at Diamond Light Source

Christoph Rau

To cite this article: Christoph Rau (2017) Imaging with Coherent Synchrotron Radiation: X-ray Imaging and Coherence Beamline (I13) at Diamond Light Source, Synchrotron Radiation News, 30:5, 19-25, DOI: 10.1080/08940886.2017.1364530

To link to this article: https://doi.org/10.1080/08940886.2017.1364530

Imaging with Coherent Synchrotron Radiation: X-ray Imaging and Coherence Beamline (I13) at Diamond Light Source

CHRISTOPH RAU
Diamond Light Source, Didcot, Oxfordshire, UK; The University of Manchester, Manchester, UK; Northwestern University, Evanston, Illinois, USA

Introduction

Synchrotron radiation provides a number of outstanding features that are highly valuable for X-ray imaging and tomography. One of them is the partial coherence of the radiation, which is explored at the X-ray Imaging and Coherence beamline (I13) at Diamond Light Source. The variety of methods employed at the beamline offer imaging with the highest quality. We discuss the benefit of imaging with coherent radiation and describe methods and applications available at Diamond's I13 beamline.

Coherent radiation at the I13 beamline

Diamond Light Source is a third-generation synchrotron light source using a 3 GeV electron storage ring to produce light for 28 operational beamlines. I13 is located in one of the long, straight sections of Diamond. The beamline I13 has two independently operated branchlines, and the experimental stations are located more than 200 m from the source. One station is dedicated to imaging in real space and called "Diamond Manchester Imaging branchline" because of the close collaboration and financial support provided by Manchester University (Figure 1, bottom, left side of graph; Figure 2, lower leg). The coherence branch applies imaging with a fully coherent beam and records data in reciprocal space (Figure 1, bottom, right side of graph; Figure 2, upper leg).

The I13 long, straight section has been modified to the so-called "mini-beta" layout (Figure 1). The long section is divided into two shorter parts by focusing magnets in the center of the section. The vertical electron beam size, which is proportional to beta function, is reduced significantly so that two insertion devices can be operated with a small gap (about 5 mm instead of 13 mm). The design provides about one order of magnitude higher photon flux compared to the original layout when used in combination with a shorter magnetic period insertion device (23 mm instead of 28 mm). The horizontal electron beam size and beta function are chosen to focus in a virtual point. For the coherence branch, this virtual source point is located in the front end of the branchline. Slits are implemented at this location so that the horizontal source size can be adjusted to the experimental needs. The slits are typically closed to a size of 50 µm; the lateral coherence length in the experimental hutch about 200 m away has been measured to be larger than 300 µm in both the horizontal and vertical directions.

To optimize the coherent flux for the coherence branch, optics such as mirrors and the monochromator are horizontally defecting to eliminate vibrations in the highly coherent vertical direction. The horizontal lateral coherence length is—as mentioned earlier—adaptable with slits installed in the front end. The coherent fraction of the radiation is selected by a set of slits in front of the experiment. The longitudinal coherence length can be adapted with the four-bounce monochromator, containing a set of Si(111) and Si(311) crystals corresponding to 0.6 µm and 5 µm longitudinal coherence length at 8 keV. The longitudinal coherence length can be fine-tuned by detuning the crystal pairs to each other. The coherent flux is about 10^{10} photons per second at 8 keV photon energy. The optical layout of the coherence branchline makes

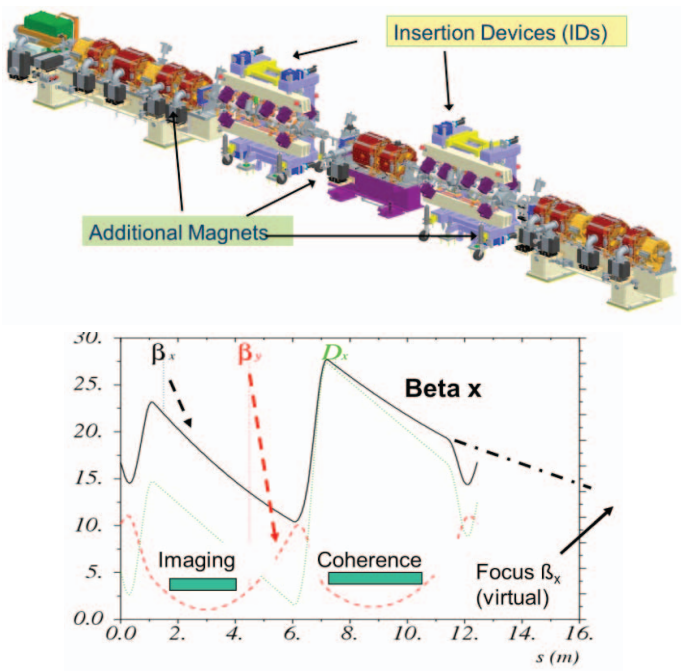

Figure 1: Scheme of "mini-beta" layout (top) and beta functions in a divided straight section (bottom). The β_x and β_y functions are proportional to the horizontal and vertical electron beam size. The green bars correspond to the length of the insertion devices.

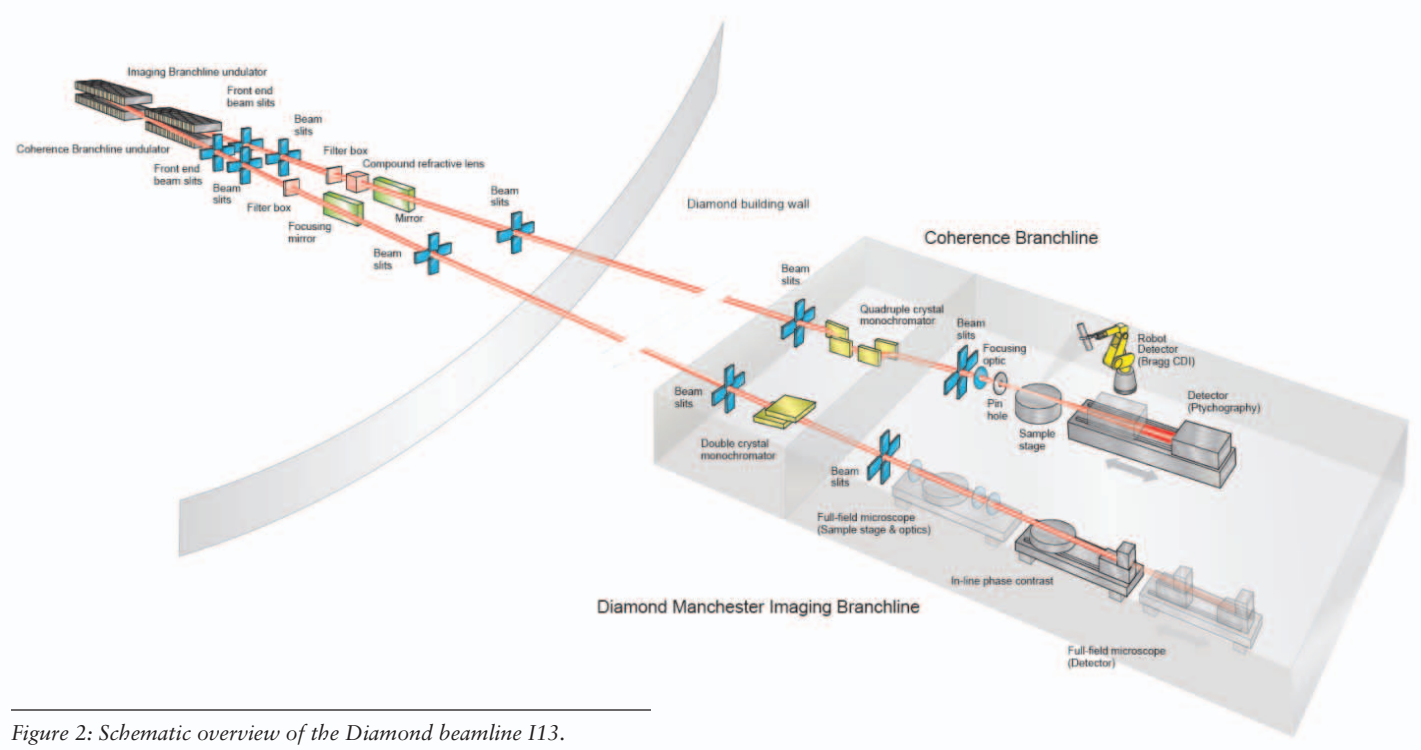

Figure 2: Schematic overview of the Diamond beamline I13.

it especially suitable for advanced imaging methods, and a series of explorative coherent optical experiments [1–5] have been conducted at the Coherence branchline of the I13 beamline.

For the Imaging branchline, the requirements for coherence are less stringent since only partial coherent radiation, if at all, is required for most experimental techniques; more details about the beamline can be found in [6].

Introduction of imaging with coherence

Conventional radiography is based on measuring the absorption of an object consisting of a given material with a thickness x and an absorption coefficient μ. The refractive index of the material describes absorption and phase shift of X-rays transmitted though the material. In the energy range around 20–30 keV, both absorption and phase shift in general are very small, but the value corresponding to the relative phase shift is about two orders of magnitude larger than the relative absorption. For this reason, it is very rewarding to exploit the phase information. The contrast may be significantly increased and therefore the radiation dose may be significantly reduced. This is not only very valuable for biomedical applications, but also for other scientific areas where, for example, imaging with temporal resolution is required. Information on both phase and amplitude are explored when imaging with the highest spatial resolution with coherent diffractive imaging (CDI) techniques, such as Bragg-CDI and ptychography. For most scientific applications at I13, the imaging methods make use of the phase information and the coherence of the radiation.

The I13 beamline at Diamond aims for imaging on micro- and nano-lengthscales in the energy range of 6–30 keV. The unique feature of the beamline is that both imaging in real and reciprocal space is available, covering a large range of spatial resolution. The coherence of the radiation is employed especially for imaging objects with features of weak contrast. The science addressed covers a large field of applications, including materials science, biomedical applications, and environmental science.

Imaging with coherent radiation on the I13 beamline

Examples of recent scientific studies showcasing the specific features of the two independently operated branchlines, Diamond-Manchester Imaging branchline and Coherence branchline, are described.

Diamond-Manchester Imaging branchline

In-line phase contrast imaging is the most commonly used method, mainly because of its ease of use. It requires partial coherent light and is based on the edge enhancement of weakly absorbing features in the near field. The resolution is given by the detector, which consists of a scintillation screen, coupled through a visible microscope to the CCD/CMoS chip of the detector, and is in the micron range. Single-distance phase retrieval is applied [7] when assuming some prior knowledge about the material components and their respective refractive index.

Both phase and amplitude information can be measured in the near field with methods under development at the beamline [9, 10]. The information is accessible by retrieving the disturbance caused by an

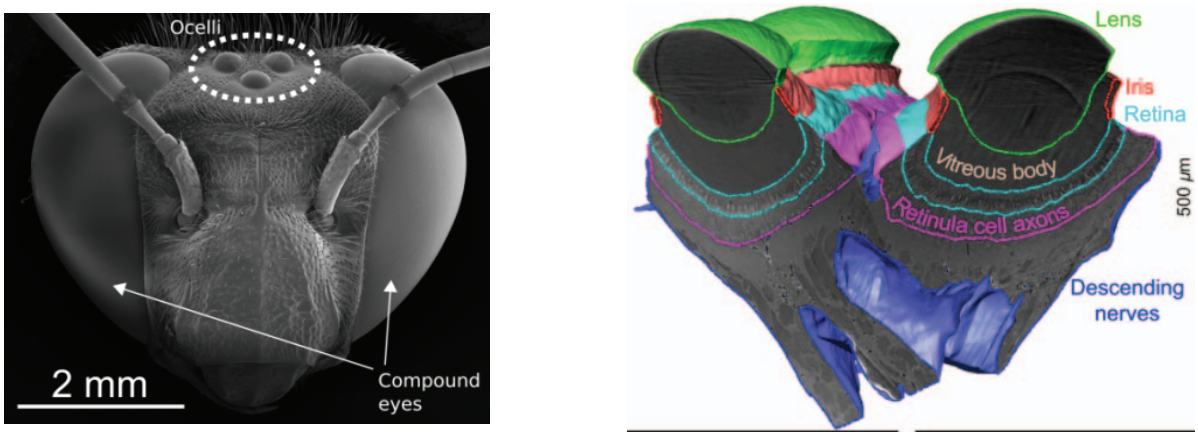

Figure 3: Image of bee head showing the area of the ocelli (left) and detailed 3D imaging achieved with in-line phase contrast microtomography (right) at I13L [8].

object on a partial coherent wavefront. This is either detected in the interference pattern generated by a grating (grating interferometry) or using objects such as sandpaper (near-field speckle). The quality of the reconstructed images is impressive and provides much ease for the segmentation using the histogram of the phase information. Figure 4 shows such a dataset recorded with grating interferometry and providing great ease for data segmentation using the phase-histogram [10].

Exploring the phase information does not necessarily require coherent radiation, which is the case for the full-field microscope, currently installed as a prototype at the beamline [11]. The instrument is primarily aiming for imaging in the 8–12 keV range with 50–100 nm spatial resolution a field of view of about 100 µm and 100 ms exposure time. An imaging method used at the Imaging branchline is the Zernike phase contrast method, which enhances contrast by manipulating the phase of diffracted (1st order) and undiffracted light (0th order) [12].

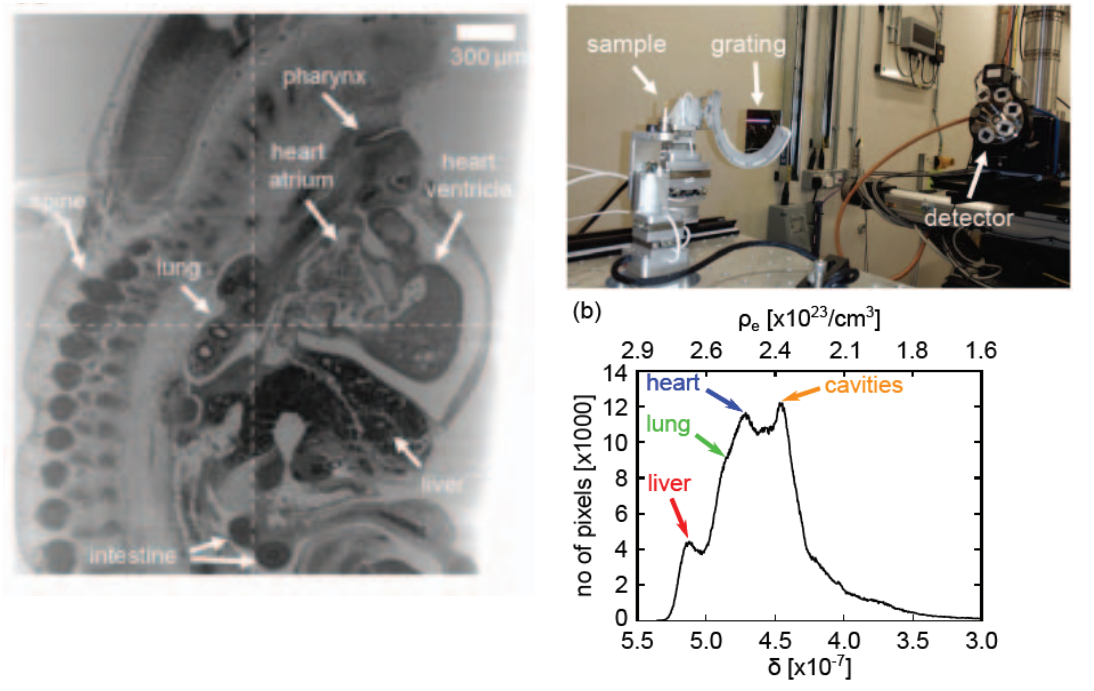

Figure 4: Experimental set-up for grating interferometry (top right), reconstructed slices and sections of mouse embryo (left), and phase-histogram for data segmentation (bottom right) [10].

Figure 5: Full-field microscopy at 8.3 keV with absorption contrast (a) and phase contrast imaging in positive (b) and negative (c) Zernike mode [11].

While the methods on the Imaging branchline operating in the near field and with partial coherent light are limited in resolution, either by the detector or the X-ray optics, on the Coherence branchline highest spatial resolution is achieved using fully coherent light.

Coherence branchline

The Coherence branchline hosts a large number of coherence-related experiments, exploring the unique radiation properties available at the beamline. Many of these experiments are explorative, while ptychography and Bragg-CDI (coherent diffractive imaging) are implemented as standard techniques for user operation.

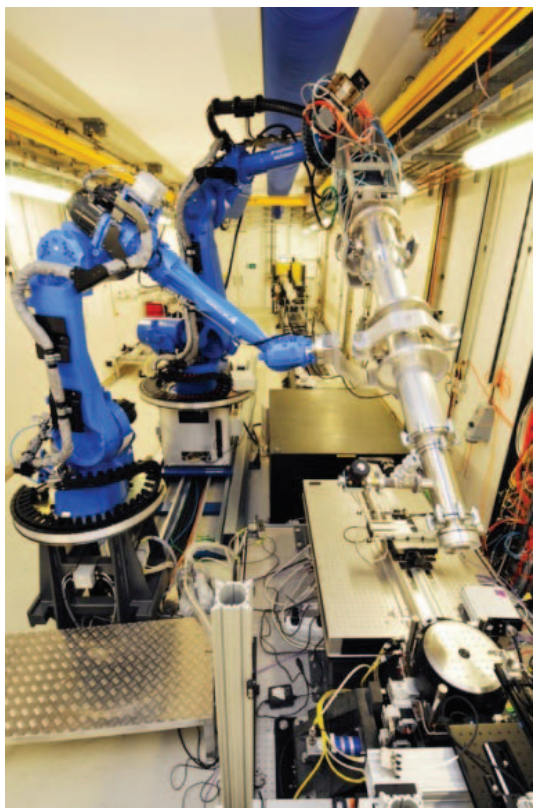

Coherence experiments

The experiments span from correcting lens aberrations with corrective optics [3], to advanced optics testing with the Ronchi method [4], and tomography with a novel beam tracking method [13]. Nano-scanning instrumentation was tested jointly with the HXN team at NSLSII, providing a 13 nm × 33 nm spot with multilayer laue lenses (MLL) for the study of chromosomes [14, 15]. The large lateral coherence length also provides new opportunities for holographic imaging [16]. We have tested new methods with variable reference objects. Current exposure times are in the order of minutes with spatial resolution of a few microns. With the proposed Diamond II machine upgrade, the exposure times will be significantly reduced and help holography become relevant for user-oriented methods. Other, more application-oriented experiments were carried out in collaboration with other facilities; for example, shearing in soft colloidal liquids was measured using a rheometer with photon correlation spectroscopy (XPCS) [17].

Ptychography and Bragg-CDI

For both ptychography and Bragg-CDI, either Fresnel zone plates (FZP) or Kirkpatrick-Baez (KB) mirrors system can be used. The useable spot size ranges from about 150 nm to 10 µm. The maximum use-

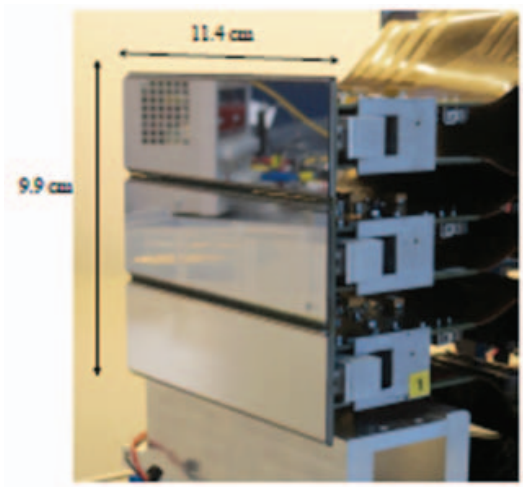

Figure 6: Instrumentation on the coherence branch: Robot arms for Bragg-CDI (left) and Diamond/STFC developed EXCALIBUR detector (right) (see [18–20]).

able hutch length is about 15 m for ptychography and up to 8 m for Bragg CDI, for working in the far field over a large range of beam spots.

Currently, the sample stage is shared for ptychography and Bragg-CDI imaging, consisting of highly precise lift and tilt stages, a low run-out air-bearing rotation stage, and X-Y-Z scanning stages on the top [18]. The current ptychography and tomography capabilities are being expanded to increase the current scanning speed from 10 Hz in to 100 Hz in the near future and beyond. For detecting the diffraction pattern photon counting, devices such as the in-house-developed MERLIN detector or the EXCALIBUR detector, developed in collaboration with STFC [19, 20], are used. The EXCALIBUR detector consists of a 6 × 8 array of 256 × 256 pixel MediPix3/3RX chips, with a 55 µm pixel size and 12-bit readout at 100 Hz continuous mode and up to 1 kHz in burst mode. In single bit mode, useful for XPCS (X-ray photon correlation spectroscopy), the detector can be operated up to 30 kHz. The arrangement of three panels with two rows of eight MediPix chips is shown in Figure 6 (right). In addition to the coherent diffraction imaging method used, it is also possible to record the fluorescence signal with a separate detector to identify chemical elements.

Ptychography experiments

The long hutch of the Coherence branchline permits using micro- and nano-beams while still satisfying the far-field condition for ptychography experiments. These experiments embrace the overarching theme of the I13 beamline—imaging on the micro- to the nano-lengthscales with coherent radiation. Many scientific applications require multi-lengthscale capability, including studying battery materials, environmental samples, and crack propagation in bones and materials. We are currently developing a scientific program for ptychography with scientific applications stemming from the imaging branch experiments and requiring this multi-scale capability.

In the early phase of the branchline development, we explored the boundaries for ptychography. While currently operating primarily with a monochromatic beam, pink beam will increase the flux by at least one order of magnitude. The recorded data need to be decomposed into different coherent "modes" [21, 22]. Further, it turns out that undersampled data, not satisfying the Nyquist condition, can be recovered for ptychographic scans [23, 24] (Figure 7). Moreover, we investigated the influence of a "diffuser" on the data quality and resolution [25]. Today, the spatial resolution achieved is 30 nm for 2D projections and more than 100 nm for tomographic data, and will be further improved in the near future. The knowledge gained from these studies will be implemented for an optimized set-up in time.

Bragg-CDI experiments

Stress and deformation of nano-crystalline samples are investigated with Bragg-CDI. For acquiring three-dimensional information, the sample is scanned around a Bragg peak under coherent illumination.

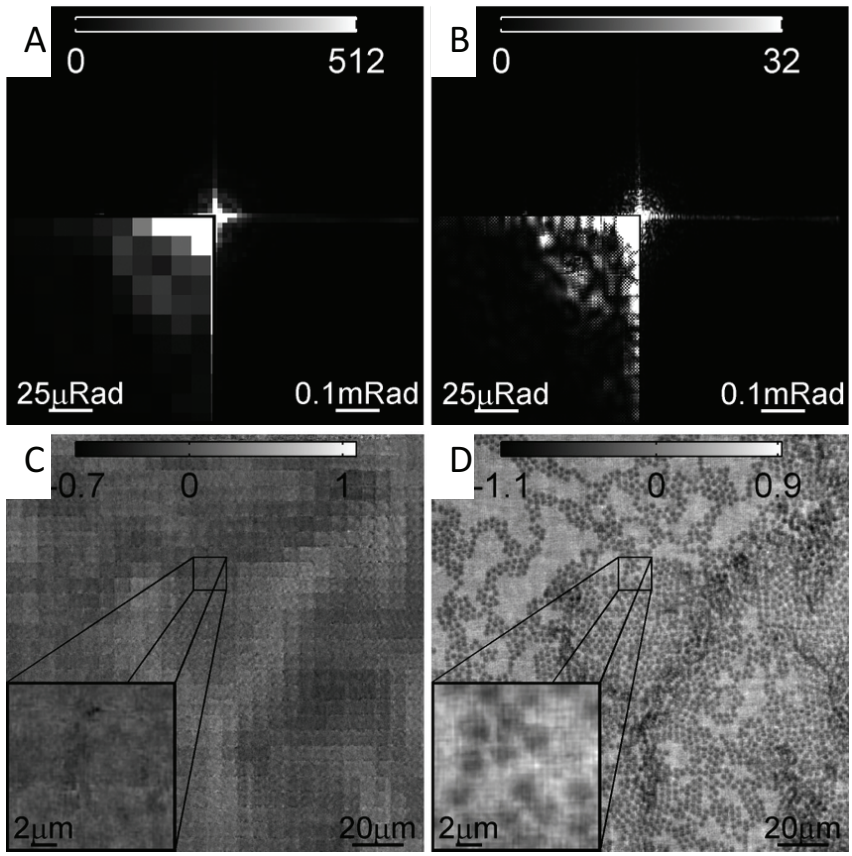

Figure 7: Ptychographic reconstructions, with magnified inlays, from a set of undersampled diffraction patterns. Images C and D show the reconstructions from the raw data shown in A (typical frame from the set) without and with the upsampling algorithm (sPIE), respectively. B shows the outputted forward model of A after the sPIE processing, with fringe visibility restored. Adapted with permission from [21]. © American Physical Society.

Data are recorded with the EXCALIBUR or the MERLIN detector, which, in turn, is positioned by a robot arm. It can reach a vertically deflected angle of 55° with a 2 m vacuum pipe in front, and is extendable to up 8 m. The pipe is held by a second robot arm; the movement of both arms is coordinated with third-party software. The drift of the system is under thermally stable conditions (now 0.1°C) in the order of several microns and only a fraction of a pixel in size [18]. The downstream view of the robot arm system is shown in Figure 6 (left).

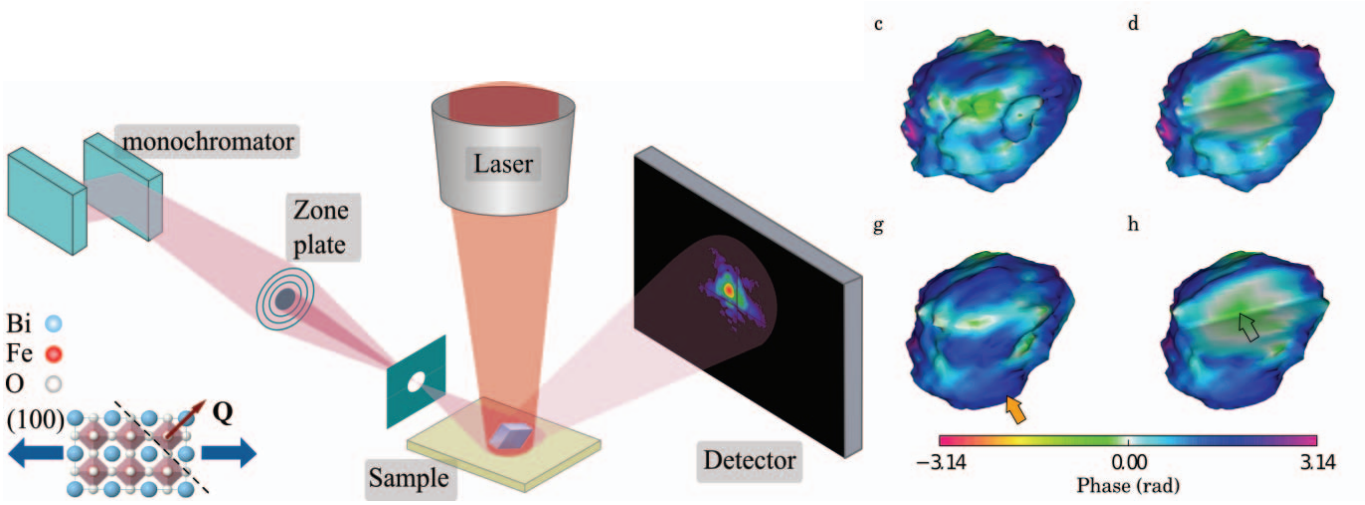

Figure 8: Experimental scheme for Bragg-CDI experiment on multiferroic bismuth ferrite (BiFeO3) (left). Representation of tensile strain on the crystal tensile strain at different stages of laser excitation (right). Adapted with permission from [24].

A typical study is the investigation of multiferroic materials, exhibiting coupling between ferroelectric and magnetic properties. They are of considerable importance for technological applications and are also interesting from a fundamental standpoint. Bismuth ferrite (BiFeO3) is one such material with room-temperature anti-ferromagnetic and ferroelectric ordering. Exciting the material with a laser induces tensile strain beyond 8×10^{-2} predominantly at the surface of the nanoscale crystal [26].

Summary and outlook

Coherent radiation provides unique opportunities for high-resolution imaging, revealing weakly absorbing structures, achieving the highest spatial resolution, and even recording data at a rapid pace. The I13 beamline exploits coherence in a suite of methods applicable over a large range of lengthscales. In the operating energy range of 6–30 keV, in situ and in operando measurements can be performed, taking advantage of the highly sensitive phase information. Radiation damage can be limited, which is particularly beneficial for biomedical applications. The experimental techniques will improve further, including, but not limited to, studies in wet environments and with higher spatial resolution. The upgrade of synchrotron sources to lower emittance machines is of obvious benefit for coherence-related imaging. The higher brilliance of the proposed Diamond-II will enable the Coherence branchline sub-10-nm resolution imaging, and on the Diamond Manchester Imaging branchline visibility of the data will be increased. Furthermore, the possibility of holography might become a method for standard user experiments [16]. Reducing the gap for insertion devices below 5 mm and shorter ID magnetic periods will provide significantly more flux and will be further enhanced with an upgraded insertion device with cryo-technology.

Acknowledgments

The I13 beamline is supported for construction and operation of the Diamond-Manchester branchline by the Diamond-Manchester collaboration. The team located at I13 consists of (in alphabetical order) Darren Batey, Andrew Bodey, Silvia Cipiccia, Shashidhara Marathe, Simon Logan, Xiaowen Shi, Malte Storm, Ulrich Wagner, Irene Zanette, Marie-Christine Zdora. Charan Kuppili, Mirna Saliba, and Simone Sala, under the guidance of Pierre Thibault, are further collaborators on coherence experiments. Ulrich Wagner contributed significantly to the optical layout in conjunction with the machine team (B. Singh, R. Bartolini). ■

References

1. L. Alianelli et al., *Proc. SPIE* **9963**, 99630 (2016).
2. P. Vagovic et al., *Optics Express* **22**(18), 21508–21520 (2014).
3. F. Seiboth et al., *Nature Communications* **8**, 14623 (2017).
4. F. Uhlén et al., *Journal of Synchrotron Radiation*, 1105–1109 (2014).
5. H. C. Wang et al., *Optics Letters* **39**(8), 2518–2521 (2014).
6. C. Rau et al., *Physica Status Solidi* (a) **208**(11), 2522–2525 (2011).
7. D. Paganin et al., *Journal of Microscopy* **206**, 33–40 (2002).
8. G. J. Taylor et al., *Current Biology* **26**(10), 1319–1324 (2016).
9. M. C. Zdora et al., *Physical Review Letters* **118**(20), 203903 (2017).
10. M. C. Zdora et al., *Biomedical Optics Express* **8**(2), 1257–1270 (2017).
11. J. Vila-Comamala et al., *XRM 2014: Proceedings of the 12th International Conference on X-Ray Microscopy* **1696**, 020036 (2016).
12. F. Zernike, *Physica* **9**(7), 686–698 (1942).
13. F. A. Vittoria et al., *Scientific Reports* **5**, 16318 (2015).
14. H. Yan et al., *Scientific Reports* **6**, 20112 (2016).
15. E. Nazaretski et al., *Journal of Synchrotron Radiation* **22**, 336–341 (2015).
16. M. Saliba et al., *Microscopy and Microanalysis* **22**, 110–111 (2016).
17. F. Westermeier et al., *Soft Matter* **12**, 171–180 (2015).
18. Z. Pešić et al., *Journal of Physics: Conference Series* **425**, 182003 (2013).
19. N. Tartoni et al., *2012 IEEE Nuclear Science Symposium and Medical Imaging Conference Record*, 530–533 (2012).
20. J. Marchal et al., *11th International Conference on Synchrotron Radiation Instrumentation* **425**, 062003 (2013).
21. P. Thibault and A. Menzel, *Nature* **494**(7435), 68–71 (2013).
22. D. J. Batey, D. Claus, and J. M. Rodenburg, *Ultramicroscopy* **138**, 13–21 (2014).
23. T. B. Edo et al., *Physical Review A* **87**(5), 053850 (2013).
24. D. Batey et al., *Physical Review A* **89**(4), 043812 (2014).
25. P. Li et al., *Journal of Optics* **18**(5), 054008 (2016).
26. M. Newton et al., *New Journal of Physics* **18**, 093003 (2016).